Soluble chromophores in marine snow, seawater, sea ice and frost flowers near Barrow, Alaska

Harry Beine, Cort Anastasio, Florent Domine, Thomas Douglas, Manuel Barret, James France, Martin King, Sam Hall, Kirk Ullmann

Soluble chromophores in marine snow, seawater, sea ice and frost flowers near Barrow, Alaska

Harry Beine,[1] Cort Anastasio,[1] Florent Domine,[2,3] Thomas Douglas,[4] Manuel Barret,[2] James France,[5] Martin King,[5] Sam Hall,[6] and Kirk Ullmann[6]

Received 29 July 2011; revised 29 January 2012; accepted 30 January 2012; published 23 March 2012.

[1] We measured light absorption in 42 marine snow, sea ice, seawater, brine, and frost flower samples collected during the OASIS field campaign between February 27 and April 15, 2009. Samples represented multiple sites between landfast ice and open pack ice in coastal areas approximately 5 km west of Barrow, Alaska. The chromophores that are most commonly measured in snow, H_2O_2, NO_3^-, and NO_2^-, on average account for less than 1% of sunlight absorption in our samples. Instead, light absorption is dominated by unidentified "residual" species, likely organic compounds. Light absorption coefficients for the frost flowers on first-year sea ice are, on average, 40 times larger than values for terrestrial snow samples at Barrow, suggesting very large rates of photochemical reactions in frost flowers. For our marine samples the calculated rates of sunlight absorption and OH production from known chromophores are (0.1–1.4) $\times$ 10^{14} (photons cm^{-3} s^{-1}) and (5–70) $\times$ 10^{-12} (mol L^{-1} s^{-1}), respectively. Our residual spectra are similar to spectra of marine chromophoric dissolved organic matter (CDOM), suggesting that CDOM is the dominant chromophore in our samples. Based on our light absorption measurements we estimate dissolved organic carbon (DOC) concentrations in Barrow seawater and frost flowers as approximately 130 and 360 μM C, respectively. We expect that CDOM is a major source of OH in our marine samples, and it is likely to have other significant photochemistry as well.

Citation: Beine, H., C. Anastasio, F. Domine, T. Douglas, M. Barret, J. France, M. King, S. Hall, and K. Ullmann (2012), Soluble chromophores in marine snow, seawater, sea ice and frost flowers near Barrow, Alaska, *J. Geophys. Res.*, *117*, D00R15, doi:10.1029/2011JD016650.

1. Introduction

[2] The absorption of sunlight by chromophores (light-absorbing species) on/in snow grains in the photic zone of the snow initiates photochemical reactions that can lead to the destruction of species in the snowpack (e.g., O_3 and organic carbon) as well as the release of a suite of compounds to the atmospheric boundary layer (e.g., NO_x, HONO, H_2O_2 and CH_2O) [*Grannas et al.*, 2007, and references therein]. To understand and quantify photochemistry in snow we must identify and quantify the major chromophores, as well as determine photon fluxes in the snowpack [*Domine and Shepson*, 2002; *Domine et al.*, 2008, and references therein]. The dominant sunlight-absorbing species in snowpacks are the ice of snow grains [*Warren and Brandt*, 2008] and insoluble impurities such as soot and soil dust [*Doherty et al.*, 2010], while soluble species such as Humic-Like Substances (HULIS) can also be important [*France et al.*, 2012; *Beine et al.*, 2011]. While sunlight absorption by ice and soot is important for the radiative balance of snowpacks, most of this absorption is at less-energetic wavelengths (i.e., at longer visible wavelengths and into the infrared) and thus probably does not lead to chemical reactions nor contribute significantly to snow photochemistry. Soluble impurities, on the other hand, account for only a small portion of the sunlight absorbed by snowpacks, but play major roles in initiating snowpack photochemistry. For example, photolysis of nitrate (NO_3^-) and nitrite (NO_2^-) in snow releases NO_x (NO + NO_2) from snowpacks, while nitrate photolysis, perhaps especially in the presence of organic/humic material, can lead to the release of HONO [*Beine et al.*, 2006, 2008; *Grannas et al.*, 2007, and references therein; *Anastasio and Chu*, 2009; *Bartels-Rausch et al.*, 2010]. However, with the exception of three major chromophores that have been identified in snow – NO_3^-, NO_2^- and H_2O_2 – we know little

[1]Department of Land, Air and Water Resources, University of California, Davis, California, USA.
[2]Laboratoire de Glaciologie et Géophysique de l'Environnement, CNRS-INSU, Université Joseph Fourier–Grenoble I, Saint-Martin d'Hères, France.
[3]Now at CNRS UMI 3376 Takuvik, Université Laval, Québec, Quebec, Canada.
[4]U.S. Army Cold Regions Research and Engineering Laboratory, Fort Wainwright, Alaska, USA.
[5]Department of Earth Sciences, Royal Holloway, University of London, Egham, UK.
[6]NCAR/ACD, Boulder, Colorado, USA.

0148-0227/12/2011JD016650

about the identities of snow-grain chromophores, their contributions to light absorption, or their chemistries.

[3] In a companion paper [*Beine et al.*, 2011] we explored soluble chromophores in 500 terrestrial snow samples collected near Barrow, AK during the Ocean – Atmosphere – Sea Ice – Snowpack (OASIS) campaign in 2009. H_2O_2, NO_3^-, and NO_2^- made minor contributions to sunlight absorption by soluble species (together accounting for <9%, typically), while HULIS and unknown chromophores each accounted for approximately half of the remaining sunlight absorption. We identified four main sources of the "residual" soluble chromophores (i.e., species other than H_2O_2 or NO_3^-) in these terrestrial snow samples: (1) species from vegetation and organic debris, which were most important in the lowest 20 cm of the snowpack, (2) marine inputs, which were associated with high Cl^- and SO_4^{2-} contents, (3) deposition of diamond dust, small ice crystals in the atmosphere that precipitate in the absence of clouds, to surface snow, and (4) gas-phase exchange between the atmosphere and surface snow layers. To complement these data on terrestrial snows, in this paper we turn our attention to marine snow, ice, brines, and frost flowers collected from the Barrow area during the same OASIS campaign.

[4] In part we are interested in frost flowers and other marine samples because of their potential roles in Arctic atmospheric chemistry. For example, springtime ozone and mercury depletion events in the Arctic are catalyzed by halogens, particularly bromine [*Barrie et al.*, 1988]. BrO is one of the key bromine species in these reactions, and BrO-rich air masses are typically of marine origin, connected to marine ices, brines, and frost flowers [e.g., *Simpson et al.*, 2007a, and references therein]. The chemical composition of frost flowers on the sea ice near Barrow and their impact on ozone and mercury chemistry is discussed by *Douglas et al.* [2012].

[5] In addition to snow on marine ice, we discuss here chromophores in seawater, nilas, sea ice, brine, and frost flowers. This is the first time that light absorption has been determined in brine and frost flower samples. Nilas, the first sea ice to form on the ocean surface in calm water, is a skim of separate crystals which initially are in the form of tiny discs, floating flat on the surface. The sea ice in our samples is first-year ice of up to 1 m thick. Brine is fractionated seawater that is transported upward through ice-grain boundaries and toward the cold ice surface by the thermomolecular pressure gradient [*Martin et al.*, 1996], where it forms slush with up to three times higher salinities than seawater [*Simpson et al.*, 2007b]. Frost flowers are feathery, delicate ice crystals that grow over refreezing sea-ice leads. They consist of a crystalline skeleton that is formed within hours by condensation on brine nodules in the cold, humid atmosphere in the marine environment [*Alvarez-Aviles et al.*, 2008; *Douglas et al.*, 2008]. Brine is continuously wicked up into the frost flower crystal lattice from the sea-ice surface (this early stage is here termed "wet frost flowers") until the brine is exhausted and the sea-ice surface dries out (resulting in "aged frost flowers," not to be confused with "dry" frost flowers that are the stage prior to wicking of brine as described in the literature [*Domine et al.*, 2005, *Douglas et al.*, 2012]); this wicking causes high concentrations of halogens and other trace species in the frost flowers. Vapor phase deposition to the frost flower surface continues, reducing the initially high major element and salinity concentrations over time (to form "old frost flowers"), and eventually the frost flowers are entrained in winds, covered by snowfall or flooded with seawater.

[6] For Barrow terrestrial samples we showed that aquatic and terrestrial humic and fulvic compounds and HULIS contribute significantly to the observed light absorption [*Beine et al.*, 2011]. Similarly, all natural waters, including ocean water contain "colored (or chromophoric) dissolved organic matter" (CDOM), which is one of the most important natural sunlight-absorbing classes in surface waters [*Zanardi-Lamardo et al.*, 2004; *Coble*, 2007, and references therein]. Historically, CDOM was first described by the oceanographic community as "yellow substance" (Gelbstoff) [e.g., *Kirk*, 1976]. Thus, the yellow color (absorption in the visible) was an essential defining attribute of these chromophores. Today, CDOM is operationally defined as the component of total dissolved organic matter (DOM) that absorbs light over a broad range of visible and UV wavelengths. The composition and structure of CDOM may be derived from aquatic and terrestrial humic and fulvic compounds, which contain lignins, phenols, and other plant degradation products, and also from polymerization of sugars, amino acids and peptides, and other small molecules in the ocean [*Coble*, 2007]. These broad classes of compounds (humics, HULIS, CDOM) are operationally defined and have somewhat different light absorbing properties, structure and composition [e.g., *Graber and Rudich*, 2006; *Green and Blough*, 1994]. The wavelength-dependent absorption coefficient of CDOM can be used to estimate a multitude of properties of a given sample. For example, it has been proposed that CDOM absorption is correlated to dissolved organic carbon (DOC) content [e.g., *Mannino et al.*, 2008], molecular weight [e.g., *Peuravuori and Pihlaja*, 1997], fluorescence [e.g., *Green and Blough*, 1994] and sources [e.g., *Helms et al.*, 2008; *Stedmon et al.*, 2011].

[7] To quantify and characterize light absorption by soluble chemical species in marine snow and ice, we recently made measurements of light absorption and soluble chromophores as part of the international, multidisciplinary Ocean - Atmosphere - Sea Ice - Snowpack (OASIS) campaign in Barrow, Alaska. We are interested in the sources, nature, and photochemistry of unidentified chromophores, especially those that absorb the most energetic wavelengths of tropospheric sunlight (which we consider here as 300 to 450 nm), as these photons likely drive snowpack photochemistry. For the OASIS campaign we had the following goals: a) determine light absorption in marine brine and frost flower samples for the first time, (b) quantify the contributions and relative importance of individual known (H_2O_2, NO_3^-, and NO_2^-) and "residual" chromophores, which appear to be mostly CDOM, (c) compare the sunlight absorption of various marine samples, (d) calculate OH production rate in these samples, and (e) consider unknown chromophores and their possible effects on polar photochemistry.

2. Methods

2.1. Sample Collection and Light Absorption Measurement

[8] We collected a total of 42 marine samples during the OASIS field campaign between February 27 and April 15,

2009 at multiple sites between landfast ice and open pack ice in coastal areas approximately 5 km west of Barrow. This set consisted of marine snow (N = 15), sea ice (10), seawater (3), brine (3), nilas (1), and frost flower (10) samples. As described by *Douglas et al.* [2012] the three frost flower types represent different stages in the continuum between wet briny sea ice with initial frost flower growth ("wet frost flowers") to further flower growth on an increasingly drying sea-ice surface ("aged frost flowers"), to flowers increasingly being coated with vapor phase deposition ("old frost flowers"). Undisturbed samples were collected as described by *Domine et al.* [2004], using polyethylene gloves to avoid contamination. Samples were collected directly into precleaned 100 mL Schott glass bottles. Air temperatures remained below −20°C during sampling. The 10 sea-ice samples described here are from a cross-section of a 1-m sea-ice slab. A slab was cut and removed from the ice, and samples were taken every 10 cm and processed as all the other samples. All samples were immediately placed at −20°C after collection and similarly stored for up to 2 days, if necessary, before measuring light absorption. We measured the light absorption coefficients of our samples using a Deuterium Lamp (D2H, WPI), a 100-cm liquid wave core guide (LWCC) (WPI) and a TIDAS 1 (J&M) spectrometer. The analytical method and data treatment are described in detail by *Beine et al.* [2011] and are only discussed briefly here. Samples were slowly melted (in the capped bottles) immediately prior to light absorption measurements. We introduced all melted samples and blanks (at room temperature) into the LWCC after filtering through an inline 0.22 μm Teflon disposable syringe filter (Cameo), and we recorded spectra between 220 and 600 nm. Before and after each sample spectrum a reference spectrum of purified water was recorded as blank. Our purified water ("MQ") was obtained from the Barrow Arctic Science Consortium's (BASC) Milli-Q Plus system (≥18.2 MΩ cm). Our measured absorption values were well above the 10-σ quantification level, which was on the order of 0.5×10^{-3} m^{-1}. Our marine spectra frequently showed a negative baseline offset at wavelengths above 500 nm; we corrected these spectra by adding the absolute value of the minimum extinction coefficient between 500 and 600 nm to the entire spectrum. The median offset for the marine spectra was 5.5×10^{-3} m^{-1}, which introduces a relative error to our spectra of less than 1% at wavelengths below 320 nm, up to 10% at 500 nm, and up to 60% at 540 nm and higher.

[9] We determined the wavelength-dependent light absorption coefficient α_λ for each sample by normalizing the measured absorbance (A_λ) of the melted sample by optical path length (l), i.e., $\alpha_\lambda = A_\lambda/l$, where the absorbance of the solution is defined as $A_\lambda = \log_{10}(I_0/I)$ at wavelength λ. As discussed by *Beine et al.* [2011], we see no evidence that scattering contributes significantly to light extinction in our samples, which were filtered.

2.2. Absorption Due to Residual Chromophores

[10] The sample light absorption coefficient (α_λ) at a given wavelength is the sum of the absorption coefficient contributions from all chromophores at that wavelength. We determined the contributions of three chromophores – nitrate, nitrite, and hydrogen peroxide – in our snow sample absorption spectra by using values of $\varepsilon_{i,\lambda}$ (the base-10 molar absorptivity of the chromophore at wavelength λ from *Beine et al.* [2011, and references therein]) and measured concentrations of NO_3^-, NO_2^-, and H_2O_2 in each sample.

[11] For each sample we determined the "residual" absorption coefficient by subtracting the NO_3^-, NO_2^-, and H_2O_2 contributions from the measured total absorption coefficient:

$$\alpha_\lambda(residual) = \alpha_\lambda - \left(\alpha_{NO3,\lambda} + \alpha_{NO2,\lambda} + \alpha_{H2O2,\lambda}\right) \quad (1)$$

[12] To simplify discussion of our results, we calculated two sums from the wavelength-dependent absorption coefficients in a given sample: (1) a sum over the full wavelength range of our measurements, i.e., 220 to 600 nm) and (2) a sum over the photochemically active wavelengths, which we consider 300 to 450 nm. In each case we summed absorption coefficients at integer wavelengths, essentially integrating over the absorption spectrum for each wavelength range [*Anastasio and Robles*, 2007]. These sums are expressed as $\Sigma\alpha_\lambda$ for the total light absorption coefficient (i.e., due to all chromophores), and $\Sigma\alpha_\lambda$(residual) for the light absorption due to all chromophores except H_2O_2, NO_2^-, and NO_3^-.

[13] Based on our spectra it appears that the residual absorption coefficient, α_λ(residual), in marine samples is dominated by colored (chromophoric) dissolved organic matter (CDOM). The composition, structure, and light absorbing properties of CDOM change significantly with the origin of the material [*Coble*, 2007]. Further, not all humic components are colored, and not all CDOM is isolated using humic substance extraction techniques. In addition, the absorption and fluorescence spectra of CDOM extracted from seawaters differ significantly from those of CDOM in the original water matrix, demonstrating that isolated CDOM is not representative of CDOM present in aquatic systems [*Green and Blough*, 1994]. Because we did not isolate CDOM in our samples, we cannot simply subtract a "CDOM" fraction from α_λ(residual), as we did for HULIS with terrestrial snow samples from Barrow [*Beine et al.*, 2011]. Our analysis (see below) therefore employs methods that are more commonly applied to oceanography. The shape of the absorption spectra of previously reported samples of CDOM from a variety of environments [*Helms et al.*, 2008] is shown in the auxiliary material (Figure S1) together with our residual spectra.[1] The strong similarity between these spectra suggests that CDOM dominates α_λ(residual) and thus we treat our α_λ(residual) spectra as CDOM spectra.

[14] The absorption coefficients of CDOM can be used to estimate a multitude of properties of the sample. For example, CDOM absorption at specific wavelengths (e.g., 275, 355, and 395 nm), is correlated with dissolved organic carbon (DOC) [*Ferrari*, 2000; *Fichot and Benner*, 2011]. Further, *Helms et al.* [2008] demonstrated that differences in the slopes of the natural log of the absorption coefficient in different wavelength ranges can be used to identify likely sources of CDOM. To perform this analysis, we determined the slope ratio (S_R) for each of our residual absorption

[1] Auxiliary materials are available with the HTML. doi:10.1029/2011JD016650.

Table 1. Characteristics of Marine Snow and Ice Samples at Barrow, Alaska[a]

Marine Samples	N	HOOH (μM)	Cl^- (mM)	Br^- (μM)	NO_3^- (μM)	NO_2^- (μM)[b]	SO_4^{2-} (mM)	$\Sigma\alpha_\lambda$ (Residual) (220–600 nm) (m^{-1})	$\Sigma\alpha_\lambda$ (Residual) (300–450 nm) (m^{-1})	Estimated DOC (μM)[c]
Surface snows	15	1.1 (±1.6)	1.9 (±2.8)	2.2 (±2.6)	3.6 (±3.2)	0.02[d]	0.16 (±0.2)	12.8 (±13.2)	2.0 (±1.6)	20
Seawater	3	0.63 (±0.04)	570 (±69)	690 (±43)	2.0 (±0.3)	0.02[e]	20.9 (±3.6)	97.6 (±1.1)	18.4 (±0.3)	130
Nilas	1	0.31	N/A	N/A	3.7	0.22	N/A	115	21.3	170
Sea Ice	10	0.12 (±0.04)	N/A	N/A	0.6 (±0.4)	0.02[f]	N/A	22.2 (±5.3)	3.9 (±1.1)	26
Brine 1	2	0.44 (±0.1)	1640 (±210)	2180 (±1)	26.0 (±5.6)	0.47 (±0.1)	70.3 (±12.3)	178 (±3.2)	44.8 (±0.1)	330
Brine 2	1	0.37	1540	1640	9.0	0.33	69.3	133	31.2	210
Frost flowers - wet	3	1.5 (±0.2)	N/A	N/A	22.1 (±11.2)	0.99 (±0.5)	0.22 (±0.2)	200 (±11)	49.8 (±1.4)	360
Frost flowers - aged	5	0.59 (±0.3)	1690 (±790)	2650 (±490)	23.9 (±5.7)	2.1 (±0.6)	39.8 (±22.4)	194 (±12.3)	48.9 (±5.2)	360
Frost flowers - old	2	4.5 (±0.0)	N/A	N/A	15.2 (±5.4)	0.37 (±0.1)	N/A	160 (±45)	37.5 (±16.7)	350

[a]Shown are mean solute concentrations (except for Nilas and Brine 2, which have only one sample each), the sum of residual absorption coefficients in the spectral ranges 220–600 nm and 300–450 nm, and estimated concentrations of DOC based on light absorption measurements. Errors are 1 standard deviation.

[b]NO_2^- concentrations are likely lower limits, as discussed in the text.

[c]Estimated average DOC concentrations for each sample type, calculated by scaling from the estimated average seawater value based on averaged light absorbance values between 250 and 400 nm (see text). It is difficult to quantify the uncertainty on these estimates, but the relative standard deviation due to sample variability should be approximately as large as the RSD value for the $\Sigma\alpha_\lambda$(residual)(300–450 nm) for that sample type. The uncertainty associated with applying the *Fichot and Benner* [2011] relationship to our samples is unknown, but is probably at least ±20%.

[d]This value was not measured, but was considered to be equal to the average Barrow terrestrial surface snow value during our campaign [*Beine et al.*, 2011].

[e]This value was not measured, but was considered to be 1% of the nitrate value, as was typical for surface seawater in the Beaufort Sea [*Simpson et al.*, 2007a].

[f]This value was not measured, but was estimated by applying the average NO_2^-/NO_3^- ratio from our other marine samples (0.036; rel. std. deviation 82%, N = 14).

spectra by dividing the slope from 275 to 295 nm by the slope from 350 to 400 nm:

$$S_R = \frac{slope\ \alpha(\text{residual};\ 275-295\ \text{nm})}{slope\ \alpha(\text{residual};\ 350-400\ \text{nm})}. \quad (2)$$

2.3. Chemical Analysis

[15] Details of the chemical analyses of our samples are described by *Beine et al.* [2011]. Prior to measuring light absorption we melted the sample, removed two unfiltered aliquots, re-froze them immediately (−20°C), stored them until the end of the Barrow campaign (4/15/09), and shipped them to our laboratory in Davis. We analyzed one aliquot from each sample for H_2O_2 using HPLC [*Kok et al.*, 1995] with a detection limit of 75 nM, and one aliquot for anions using ion chromatography (IC), with a detection limit for NO_3^- of 0.77 μM. However, most of our marine samples could not be analyzed by IC because of the large interfering Cl^- content, so we typically measured nitrate and nitrite using colorimetry [*Doane and Horwath*, 2003]. Because nitrite in frozen samples may degrade during freezing and storage [*Takenaka and Bandow*, 2007; *O'Driscoll et al.*, 2008; M. Legrand, personal communication, 2011], our NO_2^- concentrations are likely lower limits.

2.4. Sunlight Absorption

[16] The sum of the product of our measured absorption coefficients (at each integer wavelength) and the corresponding actinic flux at that wavelength is approximately equal to the rate of sunlight absorption in the marine samples [*Anastasio and Robles*, 2007]:

$$Total\ rate\ of\ sunlight\ absorption \approx \sum_\lambda (I_\lambda \times \alpha_\lambda) \quad (3)$$

where I_λ is the actinic flux (photons $cm^{-2}\ s^{-1}\ nm^{-1}$) measured at Barrow during our campaign.

2.5. OH Production Rate

[17] To assess the photochemical activity in the marine samples due to known chromophores we calculated the primary production rate of OH radicals from photolysis of hydrogen peroxide, nitrate, and nitrite (reactions 4, 5a, and 6). We also investigated the photochemical production of nitrite from nitrate (reaction 5b).

$$HOOH + h\nu \rightarrow 2\ OH \quad (4)$$

$$NO_3^- + h\nu\ (+H^+) \rightarrow NO_2 + OH \quad (5a)$$

$$NO_3^- + h\nu \rightarrow NO_2^- + O \quad (5b)$$

$$NO_2^- + h\nu\ (+H^+) \rightarrow NO + OH \quad (6)$$

We calculated the OH production rate, $R_{OH,\lambda}$, for each reaction using

$$R_{OH,\lambda} = 2.303 \times I_\lambda \times \varepsilon_\lambda \times \Phi_\lambda \times i \quad (7)$$

where ε_λ is the base-10 molar absorptivity of the reactant, Φ_λ is the quantum yield for OH production, and i is the measured molar concentration of the reactant.

[18] The temperature dependent quantum yields for the above reactions in ice are: $\Phi_{H2O2\rightarrow 2OH} = 2.27 + \exp(-684/T)$ [*Chu and Anastasio*, 2005, 2008] for reaction 4 in the quasi-liquid layer; $\Phi_{HOOH\rightarrow 2OH} = 3.859 + \exp(-1244/T)$ [*Beine and Anastasio*, 2011] for reaction 4 in a solid solution; $\Phi_{NO3^-\rightarrow OH+NO2} = 3.6 + \exp(-2400/T)$ [*Chu and Anastasio*, 2003], $\Phi_{NO3^-\rightarrow NO2^-} = 0.0015 \times \exp((20/0.008314) \times$

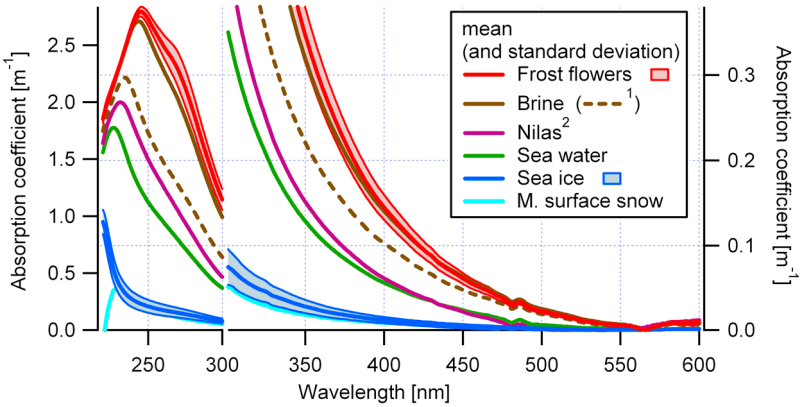

Figure 1. Mean measured absorption spectra for marine samples. The shaded areas show one standard deviation for sea-ice (N = 10) and all frost flower samples (N = 10). The *x* axis is split at 300 nm; the left *y* axis is valid for lower wavelengths, the right *y* axis for longer wavelengths. Notes: (1) Two different types of brines were observed; with sufficient difference that averaging would obscure their characteristics. (2) Only one Nilas sample was taken. M. surface snow = marine surface snow.

((1/263) − (1/T))) [*Dubowski et al.*, 2002]; $\Phi_{NO2^- \rightarrow OH}$ = (y0 + a/(1 + exp((λ − c)/b)))exp−(((eλ + f)/R) × (1/295 − 1/T)) where y0 = 0.0204, a = 0.0506, b = 11.2, c = 332, e = 20.5, f = 7553, *R* is the gas constant (8.314 J mol^{-1} K^{-1}), and λ is wavelength (nm) [*Chu and Anastasio*, 2007]. Rates of OH formation are reported in molar units (mol L^{-1} s^{-1} nm^{-1}) since this is the typical convention in the literature.

[19] Actinic fluxes at 3 m above the snow were measured at Barrow. For our OH modeling we used the mid-day actinic flux for the day the sample was taken, and mean concentrations of inorganic soluble chromophores in the marine samples (Table 1; see also *Douglas et al.* [2012] and *Domine et al.* [2011] for a further discussion of these values).

[20] We explored the possibility of estimating $R_{OH,\lambda}$ from CDOM light absorption. Measurements of OH production rates from CDOM water samples are described in the literature [e.g., *Zhou and Mopper*, 1990; *Mopper and Zhou*, 1990; *Qian et al.*, 2001; *Takeda et al.*, 2004; *Grannas et al.*, 2006] and various correlations are shown between R_{OH} and CDOM and/or DOC. However, these correlations hold for specific locations and actinic fluxes only, preventing their use to model OH production rates in our samples. We do, however, discuss these previously observed OH production rates below.

3. Results and Discussion

3.1. Marine Spectra

[21] Figure 1 shows the mean measured sample absorption spectra for our marine samples. The spectra show maximum absorption values below 245 nm and a steady, almost featureless decline with increasing wavelength to 600 nm. Values of the light absorption coefficient at 300 nm range from 0.07 m^{-1} for sea ice to 1.3 m^{-1} for frost flowers; in comparison, typical terrestrial Barrow surface snow showed an absorption coefficient on the order of 0.03 m^{-1} at 300 nm [*Beine et al.*, 2011]. Thus absorption coefficients at 300 nm

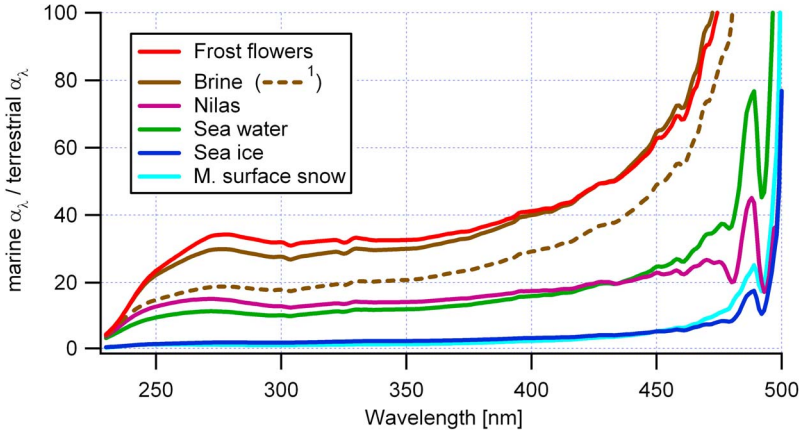

Figure 2. Ratios of measured sample absorption of marine samples to the mean terrestrial Barrow surface snow light absorption coefficient [*Beine et al.*, 2011]. Ratios beyond 500 nm are not shown, as beyond approximately 480 nm the Barrow surface snow absorption coefficients approach zero. Notes: (1) Two different types of brines were observed, with sufficient difference that averaging would obscure their characteristics. M. surface snow = marine surface snow.

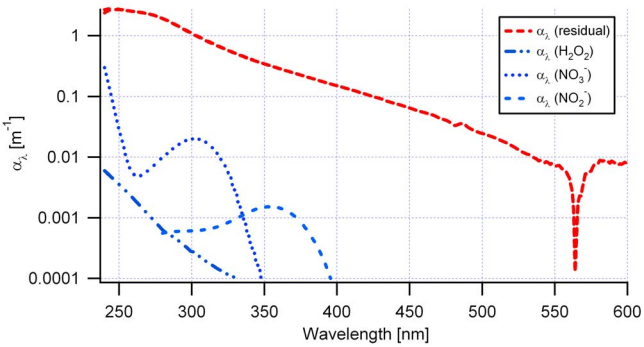

Figure 3. Residual absorption coefficient, α_λ(residual), in a sample of wet frost flowers (red line). The blue lines show the absorption coefficients for H_2O_2, NO_3^-, and NO_2^- in this sample.

in the marine samples are 2 (sea ice) to 40 (old frost flowers) times larger than values in terrestrial snow samples at Barrow. Table 1 shows the mean summed residual light absorption coefficients (i.e., $\Sigma\alpha_\lambda$(residual)) in the ice and seawater samples; recall that residual absorption coefficients have the minor contributions from H_2O_2, NO_3^-, and NO_2^- removed (section 3.2). As described below, we hypothesize that the residual light absorption (i.e., the bulk of the light absorption in the samples) is due to CDOM, although other, as yet unidentified, chromophores could also be important. Values of $\Sigma\alpha_\lambda$(residual) in our marine samples (Table 1) range from 13 to 200 m^{-1} and from 2 to 50 m^{-1} for the spectral ranges of 220–600 and 300–450 nm, respectively. For comparison, the mean (±1 relative standard deviation) values of $\Sigma\alpha_\lambda$(residual) in terrestrial surface snow samples at Barrow were 9.8 (±49%) and 1.3 (±62%) m^{-1} in these respective wavelength ranges [*Beine et al.*, 2011].

[22] Wavelength-resolved ratios of the light absorption coefficients of marine samples to the mean terrestrial Barrow surface snow values are shown in Figure 2. These ratios generally increase with wavelength, though some of the curves are nearly flat between approximately 270 and 370 nm. In the wavelength range with the greatest rates of sunlight absorption (approximately 320–420 nm; see below), light absorption coefficients for the marine samples are between 2 times (sea ice) and 45 times (frost flowers) higher than for terrestrial snow samples. Compared to the terrestrial samples, the marine samples all exhibit significantly larger absorption at long wavelengths (beyond 500 nm). This longer "tail" of the spectrum is likely due to the larger presence of light-absorbing organics in the samples (see below).

3.2. Contributions From Known Chromophores

[23] As an example of the contributions of known chromophores to light absorption, Figure 3 shows the components $\alpha_\lambda(H_2O_2)$, $\alpha_\lambda(NO_3^-)$, $\alpha_\lambda(NO_2^-)$, and α_λ(residual) in the measured light absorption spectrum of the wet frost flowers. H_2O_2, NO_3^-, and NO_2^- typically each account for 1% or less of the total light absorption coefficient at wavelengths above 250 nm. In comparison, in terrestrial snows at Summit and Dome C, Antarctica, H_2O_2 and NO_3^- were much more important, together typically accounting for 20 to 60% of sunlight absorption [*Anastasio and Robles*, 2007]. Our Barrow marine samples are much more similar to terrestrial snows at Barrow, where H_2O_2 and NO_3^- were minor components of light absorption, together contributing an average of less than 5% of the summed light absorption coefficient over 300–450 nm [*Beine et al.*, 2011]. Even though the measured concentrations of these chromophores are larger in the marine samples, the overall absorption coefficient is so much larger that the individual chromophore contributions as a percentage are smaller than in the terrestrial snow samples. For example, while the median NO_3^- concentrations in Barrow terrestrial snow and frost flowers were 3.7 μM [*Beine et al.*, 2011] and 22 μM (Table 1), respectively, NO_3^- made an insignificant (less than 1%) contribution to light absorption at wavelengths above 250 nm in both sample types. H_2O_2 and NO_2^- were also insignificant for light absorption in the marine samples and terrestrial snows, even though their concentrations were higher in the marine samples (Table 1) compared to the terrestrial snow samples (median HOOH = 0.18 μM (N = 466); average NO_2^- = 0.022 μM for a limited set of samples (N = 18) [*Beine et al.*, 2011]). However, since the marine samples were frozen and then stored for several weeks at −20°C prior to NO_2^- analysis, we are likely underestimating the nitrite concentrations and contributions.

[24] In exploring sources for chemical trace compounds, *Douglas et al.* [2012] found that α_λ(residual) generally increases as Cl^- gets enriched in marine samples, e.g., in the transition from seawater to brines to frost flowers. We do not see analogous correlations, however, for H_2O_2 or NO_3^- with sample light absorption. As shown in Figure S2, different types of samples occupy different areas in the α_λ(residual)-[chromophore] space, which indicates that seawater is not the only source for these chromophores. This is not surprising since both H_2O_2 and NO_3^- (e.g., as HNO_3) can be transferred from the atmosphere [*Hutterli et al.*, 2004; *Dibb et al.*, 2004]. The sources of chromophores and chemical composition of our frost flower samples, is further explored by *Douglas et al.* [2012].

[25] In addition to examining light absorption coefficients as described above, we also calculated rates of sunlight absorption for our marine samples. Figure 4a shows one example for the wet frost flower sample on DOY 75 (March 16); the spectral region of maximum absorption extends from approximately 320–450 nm, but there is also a large tail that extends to 600 nm, much longer (and with higher absorption) than seen for Barrow terrestrial snows [*Beine et al.*, 2011] or, especially, Summit or Dome C snows [*Anastasio and Robles*, 2007]. The total rate of sunlight absorption in this sample is 8.1×10^{13} (photons cm^{-3} s^{-1}). As shown in Figure 5, aged frost flowers and the brine samples have approximately the same value, while the old frost flowers absorb more sunlight (1.4×10^{14} (photons cm^{-3} s^{-1})). Nilas and seawater show values of approximately 4×10^{13}, and sea ice on the order of 1×10^{13} (photons cm^{-3} s^{-1}). In comparison, the maximum rate of sunlight absorption observed for Barrow terrestrial snow at DOY 100 was 3.9×10^{12} (photons cm^{-3} s^{-1}); thus the frost flowers absorb approximately 30 to 40 times more sunlight than terrestrial snow, which is broadly consistent with the ratio of light absorption coefficients between the frost flowers and terrestrial snow (Figure 2). Even the "low absorbing" marine samples also absorb much more sunlight than terrestrial snow – by factors of 2, 9, and 11 for sea ice,

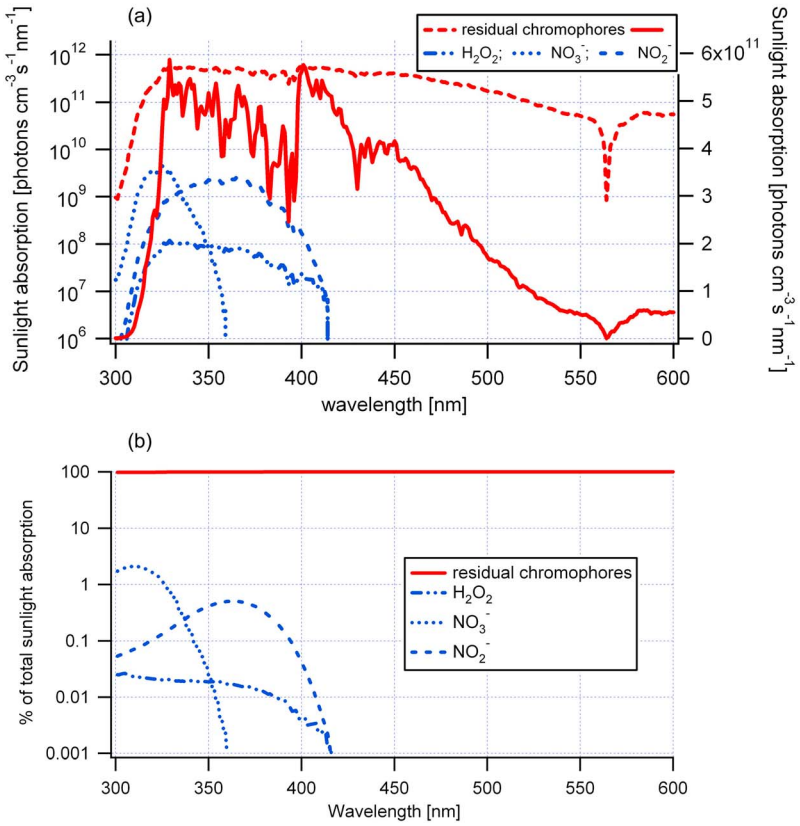

Figure 4. (a) Total sunlight absorption for sample of wet frost flowers (same sample as in Figure 3) on the day it was collected, March 16, 2009 (DOY 75) (red lines; the dashed line is for the left, logarithmic scale and the solid line is for the right, linear scale). The blue lines show the rates of sunlight absorption by H_2O_2, NO_3^-, and NO_2^- in this sample (on the logarithmic scale). (b) Percent of sunlight absorption in wet frost flowers (DOY 75) accounted for by H_2O_2, NO_3^-, and NO_2^- (blue dashed lines) and the unidentified, residual chromophores (red solid line).

nilas, and seawater, respectively – showing the great potential for photochemical reactions in these sample types.

[26] As illustrated in Figure 4b for the wet frost flowers, known chromophores make only minor contributions to sunlight absorption in our marine samples. For this sample, H_2O_2, NO_3^-, and NO_2^- contribute only 0.0075%, 0.095%, and 0.14%, respectively, to the total sunlight absorption, with maximum contributions at specific wavelengths of

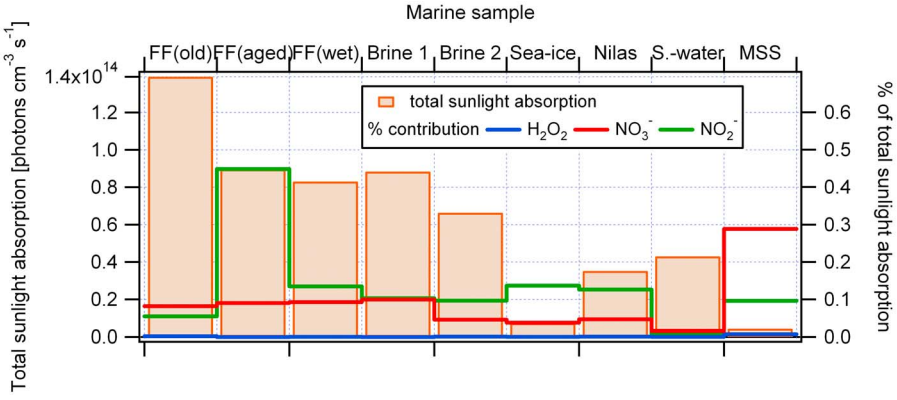

Figure 5. Calculated total rate of sunlight absorption for marine samples (tan bars, left axis). The colored lines (right axis) represent the percent contribution of known chromophores H_2O_2 (blue line), NO_3^- (red line), and NO_2^- (green line) to the sunlight absorption rate in each sample. The samples were taken between DOY 75 and DOY 97; the integrated photon flux varied on average by 20% between these dates. "MSS" = marine surface snow.

Table 2. Average Slope Ratios Calculated From the Natural Log of the Absorption Coefficients Versus Wavelength for Our Barrow Marine Samples

	Surface Snows	Seawater	Nilas	Sea Ice	Brine 1	Brine 2	Frost Flowers, Wet	Frost Flowers, Aged	Frost Flowers, Old
275–295 nm slope	−0.0013	−0.027	−0.029	−0.023	−0.026	−0.025	−0.027	−0.025	−0.028
350–400 nm slope	−0.00012	−0.016	−0.018	−0.016	−0.016	−0.015	−0.017	−0.018	−0.015
S_R	10.3	1.67	1.62	1.44	1.62	1.63	1.61	1.42	1.86

0.026% for H_2O_2 (at 301 nm), 2.1% for NO_3^- (at 309 nm), and 0.50% for NO_2^- (at 361 nm). 99.8% of the sunlight absorbed in this sample is by "residual" chromophores, which are unidentified. As shown in Figure 5, this is the case for all of our marine samples: on average, unidentified chromophores account for 99.7% of sunlight absorption, while H_2O_2, NO_3^-, and NO_2^- account for 0.002%, 0.08%, and 0.13%, respectively.

3.3. Contributions of CDOM to Light Absorption

[27] For terrestrial snow samples from Barrow we found that organic chromophores – essentially humics, fulvics, and HULIS – contributed significantly to the measured light absorption [*Beine et al.*, 2011]. In this section we explore the importance of organic chromophores in our marine samples. As shown in Figure S1, the shapes of our light absorption spectra are all similar, although the absorption coefficients in our samples vary by over an order of magnitude. Compared to CDOM spectra from midlatitude waters [*Helms et al.*, 2008], our absorption spectra have shapes that are most similar in shape to that of bay CDOM, though the magnitudes of absorption in our samples are lower and more similar to midlatitude coastal and open-ocean CDOM (Figure S1). These similarities suggest that CDOM is the dominant soluble chromophore in our samples.

[28] Following the idea of *Helms et al.* [2008], we use absorption spectra slope ratios (S_R; equation 2) to help identify possible source regions of the CDOM in our marine samples. *Helms et al.* [2008] show that values of $S_R < 1$ arise from terrestrial aquatic systems, $S_R > 1$ are associated with bays and coastal oceanic systems and S_R values approaching 10 are associated with deep open ocean waters. Similarly, *Stedmon et al.* [2011] show S_R values of approximately 20 for open Arctic Ocean surface waters. The slope ratios for our marine samples, shown in Table 2, are all between 1.4 and 1.9, suggesting that the CDOM in the Barrow ice and seawater originated from coastal marine waters, probably with terrestrial inputs from local rivers. This is consistent with *Stedmon et al.* [2011], who were able to quantify mixing from terrestrial/riverine, autochthonous, and oceanic CDOM sources in the Arctic ocean. The one outlier in our samples is marine surface snow, which has a S_R of 10, indicating a source that is different from terrestrial, riverine or surface ocean sources. For the frost flowers, values of S_R increase modestly with sample age from the wet to old samples, which is consistent with the effect of photobleaching on CDOM and its light absorption slope ratios [*Helms et al.*, 2008]. However, the aged frost flowers (which are intermediate in age) have the lowest value of S_R, which is inconsistent with the expectation that photobleaching increases S_R.

[29] To estimate DOC concentrations in our samples, we use the coastal water correlation between CDOM absorptions at 275 and 295 nm and DOC concentration that was previously applied to determine DOC concentrations of 70–400 μM C for Alaskan coastal waters [*Fichot and Benner*, 2011]. Using this correlation we estimate a DOC concentration in Barrow seawater of 130 μM, which is consistent with the broad range observed by *Fichot and Benner* [2011]. We get the same DOC level for Barrow seawater if we use the DOC/CDOM correlation developed from North Sea and Atlantic Ocean samples by *Ferrari* [2000]. Using *Fichot and Benner*'s DOC / CDOM relationship for Barrow seawater we estimate that average organic carbon concentrations are 20 μM C in marine surface snows, 26 μM C in sea ice, and up to 360 μM C in frost flowers (Table 1). Our calculated DOC values are all within, but at the upper end, of previously measured concentration ranges in comparable environments: terrestrial surface snow at Barrow contains between 8 and 25 μM DOC (D. Voisin et al., Carbonaceous species and Humic-Like Substances (HULIS) in Arctic snowpack during OASIS field campaign, submitted to *Journal of Geophysical Research*, 2012), DOC in Antarctic sea ice ranges from 1.5 to 32 μM [*Riedel et al.*, 2008], and Arctic Ocean surface waters contain 60 to 137 μM DOC [*Amon and Benner*, 2003]. In comparison, the six major rivers discharging into the Arctic basin on average contain 335 μM C during March [*Stedmon et al.*, 2011]. The increase of DOC from seawater to brines to frost flowers indicated by our data is consistent with the enrichment of many species that occurs during formation of brine and frost flowers from seawater [e.g., *Alvarez-Aviles et al.*, 2008; *Douglas et al.*, 2012]. Similarly, *Bowman and Deming* [2010] find that bacteria and particulate extracellular polysaccharides (pEPS) are increased in frost flowers and brines compared to the underlying ice surfaces. Their measurement of pEPS corresponds to 4.4 mM C in frost flowers, which is 10 times higher than our DOC estimate. However, this is not inconsistent with our frost flower DOC estimates, since we filtered our samples, which should remove the bulk of pEPS.

3.4. Photochemical Production of OH and NO_2^- From Known Chromophores

[30] Figures 6a and 6b show the wavelength-dependent OH production rates from photolysis of H_2O_2, NO_3^-, and NO_2^- in the wet frost flower sample (the same sample displayed in Figures 3 and 4). The total OH production rate in noon-time sunlight is 21×10^{-12} (mol L^{-1} s^{-1}), with photolysis of H_2O_2, NO_3^-, and NO_2^- contributing 66, 5, and 29%, respectively. Photoreaction of CDOM is another potential source of OH, but we cannot meaningfully quantify this pathway, as discussed below. Figure 7 shows the contributions of the known chromophores to OH formation in

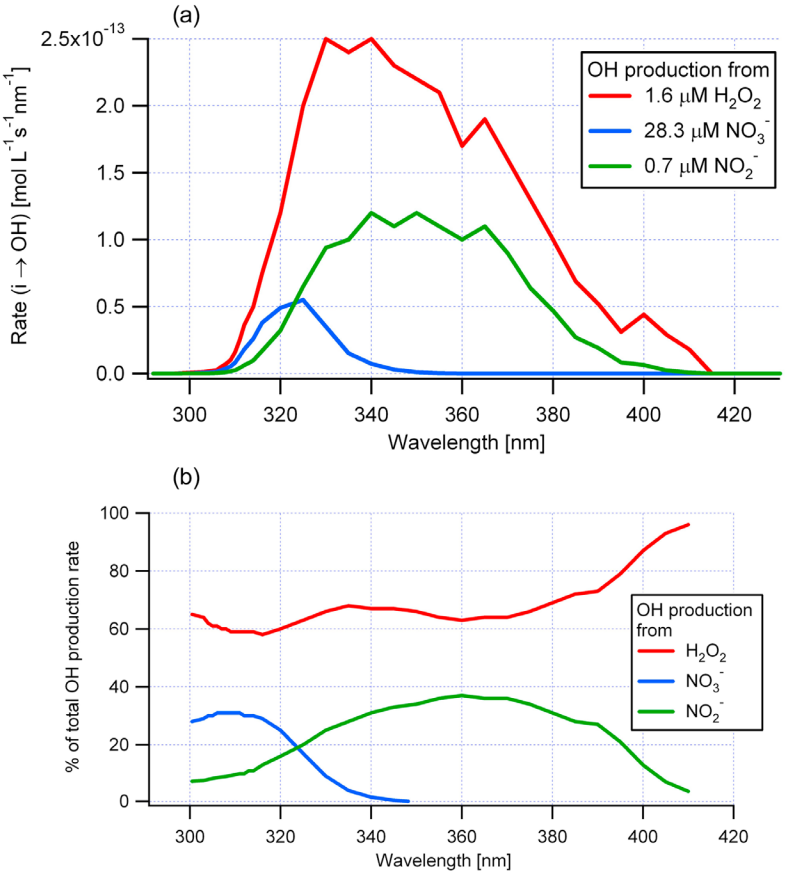

Figure 6. (a) Calculated, wavelength-resolved OH production rates from photolysis of H_2O_2 (red line), NO_3^- (blue line), and NO_2^- (green line) in the 'wet' frost flower sample on DOY 75. The total OH production rate in sunlight is 21×10^{-12} (mol L^{-1} s^{-1}). (b) Contributions from H_2O_2 (red line), NO_3^- (blue line), and NO_2^- (green line) to calculated total OH production from these chromophores in the wet frost flower sample on DOY 75.

each of the marine samples encountered at Barrow. The maximum OH production rate was 70×10^{-12} (mol L^{-1} s^{-1}) in old frost flowers, with 93% of this value due to the relatively large H_2O_2 concentration of 4.5 μM. Our marine surface snows show an average OH production of approximately 9.8×10^{-12} (mol L^{-1} s^{-1}), with H_2O_2 and NO_2^- as the dominant sources (Figure 7). This rate in surface snow is larger than the depth-integrated OH production rate from H_2O_2 in Barrow windpacks and snow on sea ice of 0.3×10^{-12} (mol L^{-1} s^{-1} for a snowpack of 10 cm depth) derived by *France et al.* [2012]. The rates are different because *France et al.* [2012] calculated a depth-integrated rate using modeled actinic fluxes from NCAR's Tropospheric Ultraviolet and Visible (*TUV*) Radiation Model and one average H_2O_2 value for all modeled snows, while we calculate surface rates from measured H_2O_2 and measured actinic flux values. *France et al.* [2007] previously estimated depth-integrated OH production rates for terrestrial snowpacks in the Canadian Arctic, Greenland, Antarctica, and Scotland, and calculated values of 0.2 to 0.6×10^{-12} (mol L^{-1} s^{-1}) due to H_2O_2 and 0.01 to 0.03×10^{-12} (mol L^{-1} s^{-1}) due to NO_3^- photolysis. *Anastasio et al.* [2007] measured typical OH production rates on surface snow grains during the summer at Summit, Greenland to be approximately 60×10^{-12} (mol L^{-1} s^{-1}), nearly all from photolysis of H_2O_2. These values are higher than our estimates for Barrow, but they were made for mid-day conditions in summer at Summit, with much higher HOOH levels (3.5–13.6 μM) in snow.

[31] We have also estimated the rate of nitrite (NO_2^-) formation from the photolysis of nitrate (NO_3^-) (equation 5b). From this simple calculation the total rate of NO_2^- production in sunlight is, on average, 3×10^{-13} (mol L^{-1} s^{-1}) for all sample types, roughly one-third of the rate of production of NO_2 and OH from nitrate photolysis. Compared to the OH production rate from all modeled reactions, nitrite photoformation is, on average, only 1.6% as large, and thus a minor process in the photochemistry of our marine samples.

3.5. OH Production From CDOM

[32] As described in section 4.3, CDOM appears to dominate sunlight absorption in our seawater, brine, frost flower, and marine snow and ice samples. Although we have not characterized the accompanying photochemical reactions of CDOM in our samples, they likely include formation of OH. CDOM is also photo- (and bio-) degraded into smaller humic-like and protein-like organic fragments and ultimately forms mainly dissolved inorganic carbon [*Coble*, 2007, and references therein]. Here we focus on OH photoformation, since that has been more studied than other CDOM pathways. Published rates of OH formation in marine waters

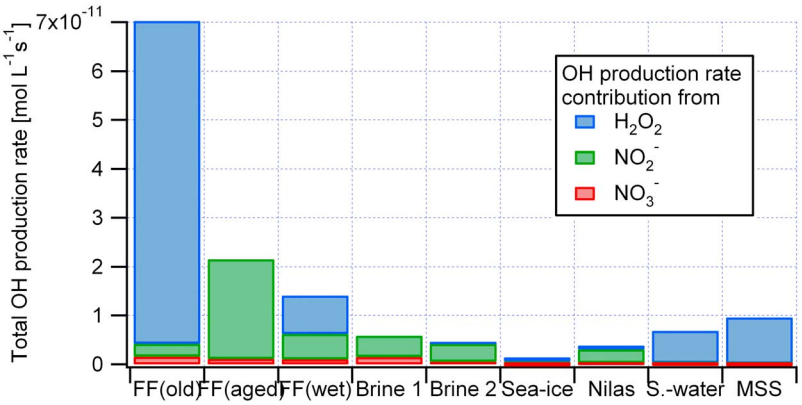

Figure 7. Mean calculated OH production rates by known chromophores, shown as stacked bars for H_2O_2 (blue), NO_3^- (red), and NO_2^- (green). FF = frost flowers, MSS = marine surface snows, i.e., snowpack on top of sea-ice. Data on individual samples, including collection dates, are listed in Table S1.

range from (0.3–0.5) $\times$ 10^{-12} (mol L^{-1} s^{-1}) for Antarctic open ocean and coastal waters [*Qian et al.*, 2001] to (32–420) $\times$ 10^{-12} (mol L^{-1} s^{-1}) for inland waters of Florida [*Zhou and Mopper*, 1990]. In the two studies where the sources of OH were examined, an "unidentified" source – likely CDOM – was by far the dominant contributor, accounting for 88% to over 95% of OH photoformation for several different midlatitude surface waters [*Mopper and Zhou*, 1990; *Takeda et al.*, 2004].

[33] We can use these data to estimate potential CDOM-derived OH production rates in our marine samples. Most simply, we first estimate rates by assuming that the production rate of OH in our Barrow seawater sample is the same as that measured for Antarctic coastal waters (0.5 $\times$ 10^{-12} (mol L^{-1} s^{-1}); *Qian et al.* [2001]) and scale this rate to the estimated DOC concentration for our other samples (Table 1). In this case, the OH production rate from CDOM photoreaction is always small (with a maximum of 1 $\times$ 10^{-12} (mol L^{-1} s^{-1}) for wet frost flowers) compared to photolysis of HOOH, NO_3^-, and NO_2^- in each sample (Figure 7). These rates are likely too low, given that CDOM dominates sunlight absorption in our samples, and that CDOM is the dominant source of OH in other surface marine waters.

[34] As a second method, we estimate CDOM-derived OH production in our Barrow samples by multiplying our estimated DOC concentrations (Table 1) by the average ratio of (CDOM-derived OH production rate) / (DOC concentration) for surface Seto Inland Sea and Yellow Seawaters from *Takeda et al.* [2004] (i.e., 0.06 $\times$ 10^{-12} (mol L^{-1} s^{-1} / μM-C)). Although only this paper reports both OH production from "unknown" chromophores and DOC levels in whole water samples, *Grannas et al.* [2006] report a similar ratio, roughly 0.02 $\times$ 10^{-12} (mol L^{-1} s^{-1} / μM-C) for DOM fractions isolated from an Alaskan lake illuminated with UV laser light. Applying the Takeda ratio results in a CDOM-derived OH production rate of 8 $\times$ 10^{-12} (mol L^{-1} s^{-1}) for Barrow seawater, which is 16 times higher than the value estimated from *Qian et al.* [2001]. Estimated rates in our other samples range from (1–2) $\times$ 10^{-12} (mol L^{-1} s^{-1}) in marine surface snows and sea ice to 20 $\times$ 10^{-12} (mol L^{-1} s^{-1}) in wet frost flowers. In all cases, these estimated rates of OH production from CDOM are comparable to the total rate from illumination of H_2O_2, NO_3^-, and NO_2^- in each sample (Figure 7). However, given that our estimates of OH production from CDOM could be an order of magnitude less than this (as described above), determining the true contribution of CDOM photoreactions in samples such as ours will require measurements of OH production.

4. Summary and Implications

[35] The chromophores that are most commonly measured in snow – H_2O_2, NO_3^-, and NO_2^- – on average account for less than 1% of sunlight absorption in our marine samples. Instead, nearly all of the light absorption in our samples is due to unidentified "residual" species that are likely dominated by chromophoric dissolved organic matter (CDOM). Light absorption coefficients for frost flowers on first-year sea ice are, on average, 40 times larger than values in terrestrial snow samples at Barrow, suggesting tremendous rates of photochemical reactions in frost flowers. A similar conclusion was made based on elevated aldehyde concentrations in frost flowers [*Douglas et al.*, 2012]. Analyzing the residual spectra as marine chromophoric dissolved organic matter (CDOM), we find that frost flowers and brines are significantly enriched in CDOM, confirming that brine expulsion and frost flower formation result in higher concentrations of chemical species. We estimate the amount of dissolved organic carbon (DOC) in Barrow seawater and frost flowers as 130 and 360 μM C, respectively.

[36] If CDOM is the main group of chromophores, as it appears, then these compounds could also be a major source of OH in our samples. Given that both bacteria and extracellular polysaccharides are elevated in frost flowers and brines compared to the underlying ice surfaces [*Bowman and Deming*, 2010], the photoformation of OH from CDOM and other chromophores likely leads to significant oxidation of these organics and, perhaps, release of volatile organic compounds to the boundary layer. Similar organic processing likely also occurs from the direct photodegradation reactions of CDOM. The high photochemical reactivity of frost flowers and brine might also impact inorganic chemistry in polar regions, e.g., the photoformed OH can oxidize bromide on snow or in solution to release gaseous

reactive bromine. In turn, these organic and inorganic reactions might impact biological processes in brine, ice, and snow.

[37] **Acknowledgments.** This work is part of the international multidisciplinary OASIS (Ocean-Atmosphere-Sea Ice-Snowpack) program. Funding for this work was gratefully received from NSF ATM-0807702. F.D. and M.B. were also funded by the French Polar Institute (IPEV grant 1017). T.D.'s research was supported by the U.S. National Science Foundation, the National Aeronautic and Space Administration, and the U.S. Army Cold Regions Research and Engineering Laboratory. J.L.F. and M.D.K. thank NERC for support through grants NE/F010788/1 and NE/F004796/1, NERC FSF for support through grant 555.0608 and the RHUL research strategy fund. We thank Tad Doane (UC Davis) for nitrate and nitrite analyses of our marine samples.

References

Alvarez-Aviles, L., W. R. Simpson, T. A. Douglas, M. Sturm, D. Perovich, and F. Domine (2008), Frost flower chemical composition during growth and its implications for aerosol production and bromine activation, *J. Geophys. Res.*, *113*, D21304, doi:10.1029/2008JD010277.

Amon, R. M. W., and R. Benner (2003), Combined neutral sugars as indicators of the diagenetic state of dissolved organic matter in the Arctic Ocean, *Deep Sea Res., Part I*, *50*(1), 151–169, doi:10.1016/S0967-0637(02)00130-9.

Anastasio, C., and L. Chu (2009), Photochemistry of nitrous acid (HONO) and nitrous acidium ion (H_2ONO^+) in aqueous solution and ice, *Environ. Sci. Technol.*, *43*(4), 1108–1114, doi:10.1021/es802579a.

Anastasio, C., and T. Robles (2007), Light absorption by soluble chemical species in Arctic and Antarctic snow, *J. Geophys. Res.*, *112*, D24304, doi:10.1029/2007JD008695.

Anastasio, C., E. S. Galbavy, M. A. Hutterli, J. F. Burkhart, and D. K. Friel (2007), Photoformation of hydroxyl radical on snow grains at Summit, Greenland, *Atmos. Environ.*, *41*(24), 5110–5121, doi:10.1016/j.atmosenv.2006.12.011

Barrie, L. A., J. W. Bottenheim, R. C. Schnell, P. J. Crutzen, and R. A. Rasmussen (1988), Ozone destruction and photochemical reactions at polar sunrise in the lower Arctic atmosphere, *Nature*, *334*, 138–141, doi:10.1038/334138a0.

Bartels-Rausch, T., M. Brigante, Y. F. Elshorbany, M. Ammann, B. D'Anna, C. George, K. Stemmler, M. Ndour, and J. Kleffmann (2010), Humic acid in ice: Photo-enhanced conversion of nitrogen dioxide into nitrous acid, *Atmos. Environ.*, *44*(40), 5443–5450, doi:10.1016/j.atmosenv.2009.12.025.

Beine, H. J., and C. Anastasio (2011), The photolysis of flash - frozen dilute hydrogen peroxide solutions, *J. Geophys. Res.*, *116*, D14302, doi:10.1029/2010JD015531.

Beine, H. J., A. Amoroso, F. Domine, M. King, M. Nardino, A. Ianniello, and J. L. France (2006), Small HONO emissions from snow surfaces at Browning Pass, Antarctica, *Atmos. Chem. Phys.*, *6*, 2569–2580, doi:10.5194/acp-6-2569-2006.

Beine, H., A. J. Colussi, A. Amoroso, G. Esposito, M. Montagnoli, and M. R. Hoffmann (2008), HONO emissions from snow surfaces, *Environ. Res. Lett.*, *3*, 045005, doi:10.1088/1748-9326/3/4/045005.

Beine, H. J., C. Anastasio, G. Esposito, K. Patten, E. Wilkening, F. Domine, D. Voisin, M. Barret, S. Houdier, and S. Hall (2011), Soluble, light-absorbing species in snow at Barrow, Alaska, *J. Geophys. Res.*, *116*, D00R05, doi:10.1029/2011JD016181.

Bowman, J. S., and J. W. Deming (2010), Elevated bacterial abundance and exopolymers in saline frost flowers and implications for atmospheric chemistry and microbial dispersal, *Geophys. Res. Lett.*, *37*, L13501, doi:10.1029/2010GL043020.

Chu, L., and C. Anastasio (2003), Quantum yields of hydroxyl radical and nitrogen dioxide from the photolysis of nitrate on ice, *J. Phys. Chem. A*, *107*, 9594–9602, doi:10.1021/jp0349132.

Chu, L., and C. Anastasio (2005), Formation of hydroxyl radical from the photolysis of frozen hydrogen peroxide, *J. Phys. Chem. A*, *109*, 6264–6271, doi:10.1021/jp051415f.

Chu, L., and C. Anastasio (2007), Temperature and wavelength dependence of nitrite photolysis in frozen and aqueous solutions, *Environ. Sci. Technol.*, *41*, 3626–3632, doi:10.1021/es062731q.

Chu, L., and C. Anastasio (2008), Addition and correction to Formation of hydroxyl radical from the photolysis of frozen hydrogen peroxide, *J. Phys. Chem. A*, *112*, 2747–2748, doi:10.1021/jp800491n.

Coble, P. G. (2007), Marine optical biogeochemistry: The chemistry of ocean color, *Chem. Rev.*, *107*, 402–418, doi:10.1021/cr050350+.

Dibb, J. E., G. Huey, D. L. Slusher, and D. J. Tanner (2004), Soluble reactive nitrogen oxides at South Pole during ISCAT 2000, *Atmos. Environ.*, *38*(32), 5399–5409, doi:10.1016/j.atmosenv.2003.01.001.

Doane, T. A., and W. R. Horwath (2003), Spectrophotometric determination of nitrate with a single reagent, *Anal. Lett.*, *36*(12), 2713–2722, doi:10.1081/AL-120024647.

Doherty, S. J., S. G. Warren, T. C. Grenfell, A. D. Clarke, and R. E. Brandt (2010), Light-absorbing impurities in Arctic snow, *Atmos. Chem. Phys.*, *10*, 11,647–11,680, doi:10.5194/acp-10-11647-2010.

Domine, F., and P. B. Shepson (2002), Air-snow interactions and atmospheric chemistry, *Science*, *297*, 1506–1510, doi:10.1126/science.1074610.

Domine, F., R. Sparapani, A. Ianniello, and H. J. Beine (2004), The origin of sea salt in snow on Arctic sea ice and in coastal regions, *Atmos. Chem. Phys.*, *4*, 2259–2271, doi:10.5194/acp-4-2259-2004.

Domine, F., A. S. Taillandier, W. R. Simpson, and K. Severin (2005), Specific surface area, density and microstructure of frost flowers, *Geophys. Res. Lett.*, *32*, L13502, doi:10.1029/2005GL023245.

Domine, F., M. Albert, T. Huthwelker, H.-W. Jacobi, A. A. Kokhanovsky, M. Lehning, G. Picard, and W. R. Simpson (2008), Snow physics as relevant to snow photochemistry, *Atmos. Chem. Phys.*, *8*, 171–208, doi:10.5194/acp-8-171-2008.

Domine, F., J.-C. Gallet, M. Barret, S. Houdier, D. Voisin, T. A. Douglas, H. J. Beine, and C. Anastasio (2011), The specific surface area and chemical composition of diamond dust near Barrow, Alaska, *J. Geophys. Res.*, *116*, D00R06, doi:10.1029/2011JD016162.

Douglas, T. A., M. Sturm, W. R. Simpson, J. D. Blum, L. Alvarez-Aviles, G. Keeler, D. Perovich, A. Biswas, and K. Johnson (2008), The influence of snow and ice crystal formation and accumulation on mercury deposition to the Arctic, *Environ. Sci. Technol.*, *42*(5), 1542–1551, doi:10.1021/es070502d.

Douglas, T. A., et al. (2012), Frost flowers growing in the Arctic Ocean–atmosphere–sea ice–snow interface: 1. Chemical composition and formation history. *J. Geophys. Res.*, *117*, D00R09, doi:10.1029/2011JD016460.

Dubowski, Y., A. J. Colussi, C. Boxe, and M. R. Hoffmann (2002), Monotonic increase of nitrite yields in the photolysis of nitrate in ice and water between 238 and 294 K, *J. Phys. Chem. A*, *106*, 6967–6971, doi:10.1021/jp0142942.

Ferrari, G. M. (2000), The relationship between chromophoric dissolved organic matter and dissolved organic carbon in the European Atlantic coastal area and in the West Mediterranean Sea (Gulf of Lions), *Mar. Chem.*, *70*(4), 339–357, doi:10.1016/S0304-4203(00)00036-0.

Fichot, C. G., and R. Benner (2011), A novel method to estimate DOC concentrations from CDOM absorption coefficients in coastal waters, *Geophys. Res. Lett.*, *38*, L03610, doi:10.1029/2010GL046152.

France, J. L., M. D. King, and J. Lee-Taylor (2007), Hydroxyl (OH) radical production rates in snowpacks from photolysis of hydrogen peroxide (H_2O_2) and nitrate (NO_3^-), *Atmos. Environ.*, *41*(26), 5502–5509, doi:10.1016/j.atmosenv.2007.03.056.

France, J. L., H. J. Reay, M. D. King, D. Voisin, H. W. Jacobi, F. Domine, H. J. Beine, C. Anastasio, A. MacArthur, J. Lee-Taylor (2012), Hydroxyl radical and nitrogen dioxide production rates, black carbon concentrations and light-absorbing impurities from field measurements of light penetration and nadir reflectivity of on-shore and off-shore coastal Alaskan snow, *J. Geophys. Res.*, *117*, D00R12, doi:10.1029/2011JD016639.

Graber, E. R., and Y. Rudich (2006), Atmospheric HULIS: How humic-like are they? A comprehensive and critical review, *Atmos. Chem. Phys.*, *6*, 729–753, doi:10.5194/acp-6-729-2006.

Grannas, A. M., C. B. Martin, Y.-P. Chin, and M. Platz (2006), Hydroxyl radical production from irradiated Arctic dissolved organic matter, *Biogeochemistry*, *78*, 51–66, doi:10.1007/s10533-005-2342-4.

Grannas, A. M., et al. (2007), An overview of snow photochemistry: evidence, mechanisms and impacts, *Atmos. Chem. Phys.*, *7*, 4329–4373.

Green, S. A., and N. V. Blough (1994), Optical absorption and fluorescence properties of chromophoric dissolved organic matter in natural waters, *Limnol. Oceanogr.*, *39*(8), 1903–1916, doi:10.4319/lo.1994.39.8.1903.

Helms, J. R., A. Stubbins, J. D. Ritchie, E. C. Minor, D. J. Kieber, and K. Mopper (2008), Absorption spectral slopes and slope ratios as indicators of molecular weight, source, and photobleaching of chromophoric dissolved organic matter, *Limnol. Oceanogr.*, *53*(3), 955–969, doi:10.4319/lo.2008.53.3.0955.

Hutterli, M. A., J. R. McConnell, G. Chen, R. C. Bales, D. D. Davis, and D. H. Lenschow (2004), Formaldehyde and hydrogen peroxide in air, snow and interstitial air at South Pole, *Atmos. Environ.*, *38*(32), 5439–5450, doi:10.1016/j.atmosenv.2004.06.003.

Kirk, J. (1976), Yellow substance (Gelbstoff) and its contribution to attenuation of photosynthetically active radiation in some inland and coastal southeastern Australian waters, *Aust. J. Mar. Freshwater Res.*, *27*(1), 61–67, doi:10.1071/MF9760061.

Kok, G. L., S. E. McLaren, and T. A. Staffelbach (1995), HPLC determination of atmospheric organic hydroperoxides, *J. Atmos. Oceanic Technol.*, *12*(2), 282–289.

Mannino, A., M. E. Russ, and S. B. Hooker (2008), Algorithm development and validation for satellite-derived distributions of DOC and CDOM in the U.S. Middle Atlantic Bight, *J. Geophys. Res.*, *113*, C07051, doi:10.1029/2007JC004493.

Martin, S., Y. Yu, and R. Drucker (1996), The temperature dependence of frost flower growth on laboratory sea ice and the effect of the flowers on infrared observations of the surface, *J. Geophys. Res.*, *101*(C5), 12,111–12,125, doi:10.1029/96JC00208.

Mopper, K., and X. Zhou (1990), Hydroxyl radical photoproduction in the sea and its potential impact on marine processes, *Science*, *250*, 661–664, doi:10.1126/science.250.4981.661.

O'Driscoll, P., N. Minogue, N. Takenaka, and J. Sodeau (2008), Release of nitric oxide and iodine to the atmosphere from the freezing of sea-salt aerosol components, *J. Phys. Chem. A*, *112*(8), 1677–1682, doi:10.1021/jp710464c.

Peuravuori, J., and K. Pihlaja (1997), Molecular size distribution and spectroscopic properties of aquatic humic substances, *Anal. Chim. Acta*, *337*(2), 133–149, doi:10.1016/S0003-2670(96)00412-6.

Qian, J., K. Mopper, and D. J. Kieber (2001), Photochemical production of the hydroxyl radical in Antarctic waters, *Deep Sea Res., Part I*, *48*, 741–759, doi:10.1016/S0967-0637(00)00068-6.

Riedel, A., C. Michel, M. Gosselin, and B. LeBlanc (2008), Winter–spring dynamics in sea-ice carbon cycling in the coastal Arctic Ocean, *J. Mar. Syst.*, *74*(3–4), 918–932, doi:10.1016/j.jmarsys.2008.01.003.

Simpson, W. R., et al. (2007a), Halogens and their role in polar boundary-layer ozone depletion, *Atmos. Chem. Phys.*, *7*(16), 4375–4418, doi:10.5194/acp-7-4375-2007.

Simpson, W. R., L. D. Carlson, G. Honninger, T. A. Douglas, M. Sturm, D. Perovich, and U. Platt (2007b), First-year sea ice contact predicts bromine monoxide (BrO) levels at Barrow, Alaska better than potential frost flower contact, *Atmos. Chem. Phys.*, *7*, 621–627, doi:10.5194/acp-7-621-2007.

Stedmon, C. A., R. M. W. Amon, A. J. Rinehart, and S. A. Walker (2011), The supply and characteristics of colored dissolved organic matter (CDOM) in the Arctic Ocean: Pan Arctic trends and differences, *Mar. Chem.*, *124*, 108–118, doi:10.1016/j.marchem.2010.12.007.

Takeda, K., H. Takedoi, S. Yamaji, K. Ohta, and H. Sakugawa (2004), Determination of hydroxyl radical photoproduction rates in natural waters, *Anal. Sci.*, *20*, 153–158, doi:10.2116/analsci.20.153.

Takenaka, N., and H. Bandow (2007), Chemical kinetics of reactions in the unfrozen solution of ice, *J. Phys. Chem. A*, *111*(36), 8780–8786, doi:10.1021/jp0738356.

Warren, S. G., and R. E. Brandt (2008), Optical constants of ice from the ultraviolet to the microwave: A revised compilation, *J. Geophys. Res.*, *113*, D14220, doi:10.1029/2007JD009744.

Zanardi-Lamardo, E., C. A. Moore, and R. G. Zika (2004), Seasonal variation in molecular mass and optical properties of chromophoric dissolved organic material in coastal waters of southwest Florida, *Mar. Chem.*, *89*, 37–54, doi:10.1016/j.marchem.2004.02.018.

Zhou, X., and K. Mopper (1990), Determination of photochemically produced hydroxyl radicals in seawater and freshwater, *Mar. Chem.*, *30*, 71–88, doi:10.1016/0304-4203(90)90062-H.

C. Anastasio and H. Beine, Department of Land, Air and Water Resources, University of California, One Shields Avenue, Davis, CA 95616, USA.

M. Barret, Laboratoire de Glaciologie et Géophysique de l'Environnement, CNRS-INSU, Université Joseph Fourier–Grenoble I, F-38402 Saint-Martin d'Hères CEDEX, France.

F. Domine, CNRS UMI 3376 Takuvik, Université Laval, Pavillon Alexandre Vachon, Québec, QC G1V 0A6, Canada.

T. Douglas, U.S. Army Cold Regions Research and Engineering Laboratory, PO Box 35170, Fort Wainwright, AK 99703, USA.

J. France and M. King, Department of Earth Sciences, Royal Holloway, University of London, Egham Hill, Egham TW20 0EX, UK.

S. Hall and K. Ullmann, NCAR/ACD, 3090 Center Green Dr., Boulder, CO 80301, USA.